

Article

Effect of Low Concentration of SiO₂ Nanoparticles on Grape Seed Essential Oil/PBAT Composite Films for Sustainable Food Packaging Application

Soundhar Arumugam ^{1,*} , Jayakrishna Kandasamy ² , Thendral Thiyaku ^{3,*}  and Prateek Saxena ⁴ ¹ Department of Mechanical Engineering, Indian Institute of Technology, Guwahati 781039, India² School of Mechanical Engineering, VIT University, Vellore 632014, India; mail2jaikrish@gmail.com³ Department of Printing and Packaging Technology, Anna University, Chennai 600025, India⁴ School of Engineering, Indian Institute of Technology, Mandi 175005, India; prateek@iitmandi.ac.in

* Correspondence: soundhar1372214@gmail.com (S.A.); thendralannauniversity@gmail.com (T.T.)

Abstract: Active packaging material has been used in the food industry to maintain the quality of packaged foods. The use of conventional polymers has serious environmental consequences due to improper disposal or recycling methods. Therefore, active packaging films based on biopolymers have been developed due to their excellent biocompatibility, degradability, and eco-friendliness. Amongst all essential oils, grape seed oil is considered to be a promising antimicrobial agent. It comprises large quantities of flavonoids, tocopherols, and other antimicrobial compounds. Grape seed essential oil has good antimicrobial and antioxidant activity. As a film, it is used to preserve food items such as poultry products, fish, and tomatoes. This work aimed to develop a polybutylene adipate terephthalate (PBAT) biocomposite film incorporated with natural grape seed essential oil (GEO) in addition to silica nanoparticles (SiO₂ NPs) using the solution casting process. To achieve the desired packaging properties of the prepared PBAT-based film, the concentrations of grape seed essential oil as a plasticizer and nanosilica as a filler material were varied. The optical, physical, barrier, mechanical, surface hydrophobicity, and antibacterial properties of the PBAT/GEO/SiO₂NP films were assessed. The FT-IR and XRD results indicated that GEO had effective miscibility with the PBAT/SiO₂NP matrix. The addition of GEO increased the film flexibility, opacity, and antimicrobial activity, but the incorporation of SiO₂NPs in the PBAT/GEO blend increased the tensile strength, thermal stability, and antimicrobial activities. The PBAT/GEO/SiO₂NP films exhibited excellent antibacterial activity against food spoilage microorganisms. Finally, due to improved antimicrobial activities, film flexibility, optical, and heat resistance properties, the PBAT/GEO/NP nanocomposite films were found to have high potential for usage in active food packaging applications.

Keywords: active food packaging; antibacterial activity; essential oils; PBAT; silica nanoparticles; nanocomposite film



check for updates

Citation: Arumugam, S.; Kandasamy, J.; Thiyaku, T.; Saxena, P. Effect of Low Concentration of SiO₂ Nanoparticles on Grape Seed Essential Oil/PBAT Composite Films for Sustainable Food Packaging Application. *Sustainability* **2022**, *14*, 8073. <https://doi.org/10.3390/su14138073>

Academic Editors: Konstantinos S. Triantafyllidis and Mariateresa Lettieri

Received: 30 April 2022

Accepted: 29 June 2022

Published: 1 July 2022

Publisher's Note: MDPI stays neutral with regard to jurisdictional claims in published maps and institutional affiliations.



Copyright: © 2022 by the authors. Licensee MDPI, Basel, Switzerland. This article is an open access article distributed under the terms and conditions of the Creative Commons Attribution (CC BY) license (<https://creativecommons.org/licenses/by/4.0/>).

1. Introduction

As the world's population grows each year, this growth results in huge demands for food and food packaging. Food's shelf life can be extended by protecting it from the numerous harmful hazards, which is achieved with packaging materials. Additionally, these packaging materials aid the safe transportation and storage of food products [1–3]. The quality of packaged foods is maintained by using existing or new techniques in the current packaging technologies. The current approaches include modified controlled atmospheric packaging (CAP), atmospheric packaging (MAP), vacuum packaging (VP), and active intelligent packaging, which are emerging as novel methods [4,5]. Advanced technologies, such as active packaging, have recently bettered traditional food packaging technologies. The long-term safety and freshness of food, without any external packaging hazards, are maintained through these technologies [6]. The main functions of food

packaging are to maintain the quality, safety, and shelf life of food from the time it is manufactured to the time it is consumed [7]. The main causes of food decay during the specified time period are microbial contamination, lipid oxidation, enzymatic reaction, and hydrolysis [8]. Food spoilage can cause a variety of health issues; thus, there is an increasing demand for food products that can maintain their quality for an extended period of time. Because of health concerns, consumers do not always prefer to extend the service life of goods by adding chemical preservatives [9,10]. To overcome these issues, the current research mainly focuses on the use of biopolymers, natural preservatives such as antioxidants, and antibacterial agents and the incorporation of nanofillers to improve the properties of biopolymers [11–13]. The use of non-biodegradable conventional flexible polymer materials seems to have serious environmental consequences [14]. Hence, to minimize these environmental problems, the development of biobased, polymer-based packaging materials has become a global concern in recent years. In the field of food packaging, various types of biopolymers are used. Among them, polybutylene adipate terephthalate (PBAT) is considered a good replacement for synthetic plastic materials due to its highly ductile nature and its complete biodegradability, but it does not provide resistance to different microbial growths [15–17]. The development of biopolymer films infused with essential oils and nanoparticles is a growing trend in the improvement of packaging performance properties such as mechanical, barrier, antibacterial, and thermal properties in various fields of food packaging applications [18–20]. Previous researchers have investigated composite films with nanocellulose/grape seed essential oil (GEO) and immobilized silver nanoparticles (NPs), polycaprolactone films incorporated with GEO as an antimicrobial agent, chitosan films with GEO, PBAT/PLA blends incorporated with GEO, LDPE/GEO, and PBAT/GEO composite films for controlling microbial growth in fresh cheese packaging, and carrageenan incorporated with GEO for active packaging and found that composite films containing GEO had a good plasticizing effect and antibacterial activity [21–27]. The primary objective of this study was to develop active PBAT-based composite films by incorporating GEO as a plasticizer and antimicrobial agent, as well as silica NPs as nanofillers. The bioactive PBAT film was characterized using various analytical studies. The effect of GEO and SiO₂NPs on different physical (FT-IR, XRD, and film morphology) and packaging functional (oxygen, water permeability, mechanical, optical, surface wettability, and thermal stability) properties of the nanocomposite films were investigated. Furthermore, the antibacterial activity of the prepared PBAT-based films was analyzed using a disc diffusion method against food pathogenic microorganisms such as *E. coli* and *S. aureus*. According to the findings, PBAT/GEO/SiO₂ composite films can be used as antimicrobial, biobased flexible films to extend the shelf life of packaged products.

2. Materials and Methods

2.1. Materials

M/s BASF Ltd., Tokyo, Japan, supplied the biodegradable PBAT resin (142,000 g·mol⁻¹) for this work. Initially, the PBAT granules were dried out in a hot oven (at 60 °C for 4 h). Sigma Aldrich, Burlington, MA, USA, provided the SiO₂ nanoparticles with particle sizes ranging from 30 to 40 nm and the liquid chloroform. Pure (100%) and natural grape seed essential oil was procured from Cyrus Enterprises Pvt. Ltd., Chennai, India.

2.2. Preparation of PBAT/GEO/SiO₂ Nanocomposite Film

A solvent casting technique was used to develop the PBAT/GEO composite films with various types of NPs, as shown in Figure 1. As a base biopolymer, PBAT was kept at 4 gm, with varying percentages of GEO (plasticizer), and 1 and 3% SiO₂ nanoparticles was used as a nanofiller. To prepare a uniformly distributed solution, SiO₂NPs were dissolved in 100 mL of liquid chloroform and placed inside a water bath sonicator for 5 min. Subsequently, using a magnetic stirrer, different weight percentages (wt%) of biopolymer resins were mixed in the distributed NP solution by varying the concentrations of GEO, and they were allowed to dissolve for 4 h at an ambient temperature of 23 °C. A pure

PBAT film was made without grape seed oil or NPs with the same process. The transfer of the film-forming solution was poured into a Petri plate, distributed uniformly with a bending glass rod, and allowed to dry at room temperature for approximately 24 h to allow the composite films to fully cure. The desiccated composite and nanocomposite films were carefully taken from the casting plate and kept in a humidity chamber for at least 48 h (temperature = 25 °C) and 50% relative humidity. The resulting composite and nanocomposite film names are provided in Table 1. The thickness of all the prepared PBAT films was around 80–90 microns.

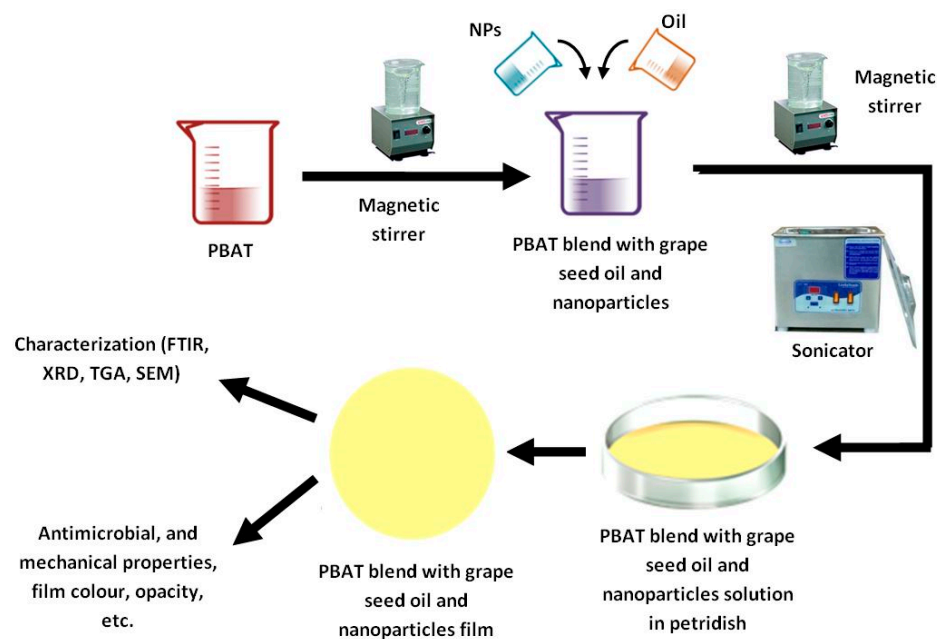


Figure 1. PBAT/GEO/SiO₂ nanocomposite film schematic illustration.

Table 1. PBAT/GEO/SiO₂ nanocomposite film formulation.

Formulated Films	Sample Code	Composition		
		PBAT (wt%)	Grape Seed Oil (wt%)	Nanosilica (wt%)
PBAT	Sample A	100.0	0.0	0.0
PBAT/GEO (95:5:0)	Sample B	95.0	5.0	0.0
PBAT/GEO (90:10:0)	Sample C	90.0	10.0	0.0
PBAT/GEO/SiO ₂ NP (89:10:1)	Sample D	89.0	10.0	1.0
PBAT/GEO/SiO ₂ NP (87:10:3)	Sample E	87.0	10.0	3.0

2.3. Characterizations

2.3.1. FTIR Analysis

Fourier transform infrared spectroscopy with the ATR approach was used to determine the presence of functional groups of PBAT/GEO/nanocomposite films using a Perkin Elmer spectrophotometer RX1 device. Tiny pieces of film specimens (2 cm × 2 cm) were extracted and placed into a specimen holder. Subsequently, infrared beams were passed to penetrate through an assortment of composite film samples, and spectral values ranging from 4000 to 400 cm⁻¹ were noted.

2.3.2. XRD Analysis

X-ray diffraction analysis (XRD) was carried out using a Mini Flex 120 II-C machine to detect the peak intensities of the fabricated PBAT/GEO/NP nanocomposite films. The tiny film specimens were mounted and scanned in the XRD analyzer (diffraction range = 5.0 to 40.0° and at 10 steps per degree).

2.3.3. Morphological Study

SEM (S-4800, Hitachi, Japan) at 5.0 kV and HRTEM (FEI Tecnai F200) at 200 kV were deployed to examine the surface, inner microstructures, and dispersion of oil droplets of PBAT/GEO/nanocomposite films. The film specimens were surface coated using gold before examining the structure. At the end of the process, high-quality and highly magnified images were taken.

2.3.4. TGA Analysis

A thermogravimetric analyzer (TGA Q500, TA Instrument, Inc., New Castle, DE, USA) was employed to find the thermal stability of the nanocomposite films. The fabricated nanocomposite films were heated at a rate of 10 °C/min (in a nitrogen environment: 50 mL/min) at temperatures ranging from 10 to 600 °C. Finally, a chart was prepared to connect temperature and weight loss using an empty alumina crucible.

2.3.5. Mechanical Properties

A computer-integrated UTM (Tinius 50 Olsen H10KS, Redhill, UK) was used to assess the mechanical characteristics of PBAT/GEO/nanocomposite films. The films (25.4 mm × 150 mm) were used to conduct the test, and the speed range of 50 mm/min was used, as per ASTM D-882-88. To identify the precise elongation of the PBAT/GEO composite films, the gauge length (50 mm) was maintained. The repeatability of the results was observed by using three specimens for testing.

2.3.6. Barrier Properties

An oxygen permeability tester (NoselabAts, Nova Milanese, Italy) and water vapor transmittance tester (Lyssy L80–5000) were employed to assess the OP and water vapor permeability (WVP) values of the fabricated PBAT/GEO/nanocomposite films. At the start, the fabricated film specimens were extracted into 30 mm (WVTR) and 55 mm (OTR) diameters and kept between the inside and outside chambers in the apparatus. The test was performed at a temperature of 25 °C with a relative humidity of 90% and 0%, as per ASTM D-3985 for OTR and ASTM F1249-90 for WVTR measurement. The repeatability of the results was observed by using three specimens for testing.

2.3.7. Optical Properties of Film

The optical properties of the PBAT/GEO/nanocomposite films were identified using a spectrophotometer instrument (X Rite528) as per ASTM D2244 (film color) and ASTM E284 (opacity). The color variation and opacity in all the fabricated films were computed with the reference of color values and a control of the PBAT film's opacity.

2.3.8. Water Contact Angle of Film

A goniometer (KSV CAM 200, KSV Instruments, Helsinki, Finland) integrated with image analysis software (DIGIDROP) was utilized to observe the wettability of the prepared films. Within the setup of a horizontal movable steel plate attached to a contact angle meter, the extracted tiny film was kept. The digital camera captured and measured the contact angle between the film's surface and the droplet after placing a drop of water in various places on the film surface. In the end, the average was computed, and the uncertainty was kept within $\pm 1^\circ$.

2.3.9. Antimicrobial Activity

The antimicrobial activity of the prepared nanocomposite films was examined using the zone of inhibition method (ISO 22196) against Gram-positive (*E. coli*) and Gram-negative (*S. aureus*) microbes. To determine antibacterial activity, all the fabricated film specimens were kept on a plate with the suspension of bacteria. The measurement of the diameter of the inhibited region around the film disc was carried out. The plates were analyzed for

potential clear regions after 48 h at 37 °C. From the observation of the inhibited zone, the antimicrobial activity of the different fabricated films was examined.

3. Results and Discussion

3.1. FTIR Analysis

The important functional groups associated with PBAT are as follows: In Figure 2A, it is shown that a broad peak around 2960 cm^{-1} was attributed to the presence of C-H in aromatic and aliphatic molecules; a peak at 1700 cm^{-1} represented carbonyl groups (C=O) in an ester linkage; and a peak at 720 cm^{-1} denoted the availability of a methylene group (-CH₂-) in the PBAT polymer [27]. Similarly, Figure 2B,C show the FT-IR spectra of PBAT/GEO composite films. When grape seed oil was utilized as a plasticizing agent in PBAT film samples (B and C), it formed peaks at 1600 cm^{-1} and 2900 cm^{-1} , denoting the presence of fatty acid and phenolic chemical compounds in GEO containing PBAT polymers [28]. However, as the concentration of GEO increased, several peaks moved to lower and higher frequencies [23]. For instance, the peaks at 2930 , 1371 , and 1074 cm^{-1} were moved to 2937 , 1375 , and 1071 cm^{-1} in the PBAT/GEO-blended film with a high concentration of GEO (10%). Similarly, Figure 2D,E show that the vibrations of the -OH and Si-O-Si groups in SiO₂ NPs prompted the absorption peaks at 1100 cm^{-1} and 1600 cm^{-1} in the FTIR spectra plots attributed due to the interlinkage of the -COO group in PBAT and SiO₂ NPs through metal bonding [26]. It was evinced that additional peaks are shown in PBAT/GEO/1% and the 3% SiO₂ nanocomposite film. When compared to the control PBAT film, additional peaks were identified and confirmed the chemical interaction in all other designated film samples of PBAT/GEO and PBAT/GEO/SiO₂ NPs. Finally, the FTIR result suggested that GEO and SiO₂ NPs have good compatibility with PBAT biodegradable polymers.

3.2. XRD Analysis

Figure 3 exhibits the XRD plots of pure PBAT, PBAT/GEO, and PBAT/GEO/SiO₂ nanocomposite films. The changes in the crystalline structure of the PBAT, PBAT/GEO, and PBAT/GEO/SiO₂ films were studied with X-ray diffraction (XRD). Figure 3 exhibits the XRD curves of PBAT/GEO/SiO₂ blends. In Figure 3A, it is shown that the pure PBAT exhibited the diffraction peaks at $2\theta = 16.5^\circ$, 17.9° , and 20° , respectively, due to the semi-crystalline nature of PBAT [29], whereas GEO incorporation in PBAT film samples (B) and (C) has caused a slight shoulder at 17.3° and produced the peak a little broad in comparison with pure PBAT film [30]. The presence of SiO₂NPs in the polymer matrix was confirmed by a peak at 23° and 24.7° in samples (D) and (E), which was attributable to the crystalline nature of nanosilica [31]. The percentage crystallinity of all the prepared film samples was calculated using Origin pro and is listed in Table 2. The percentage crystallinity of the PBAT films varied from 12.31 to 19.74. The crystallinity of the control film was 12.31, which was higher than that of the PBAT/GEO composite film. The incorporation of GEO into the PBAT film significantly reduced the crystallinity of the composite films, which could be attributed to the amorphous nature of GEO, whereas the crystallinity of the PBAT/GEO/SiO₂NP nanocomposite film significantly increased when compared to the pure PBAT film. This could be due to the crystalline nature of silica nanoparticles.

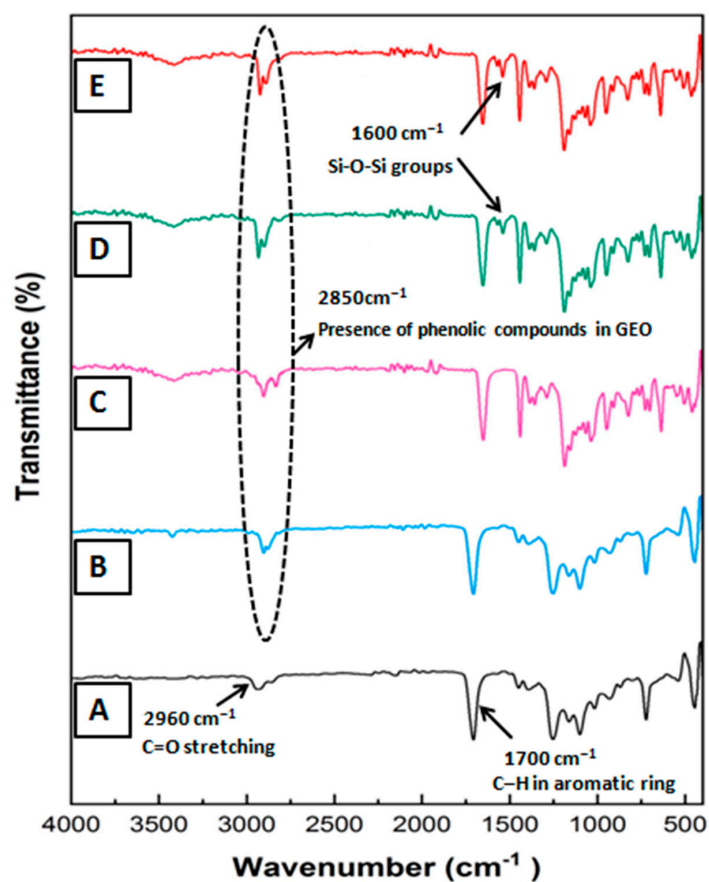


Figure 2. FTIR spectra of (A) pure PBAT film, (B) PBAT/5% of GEO composite film, (C) PBAT/10% of GEO composite film, (D) PBAT/10% of GEO/1% of SiO₂ nanocomposite film, (E) PBAT/10% of GEO/3% of SiO₂ nanocomposite film.

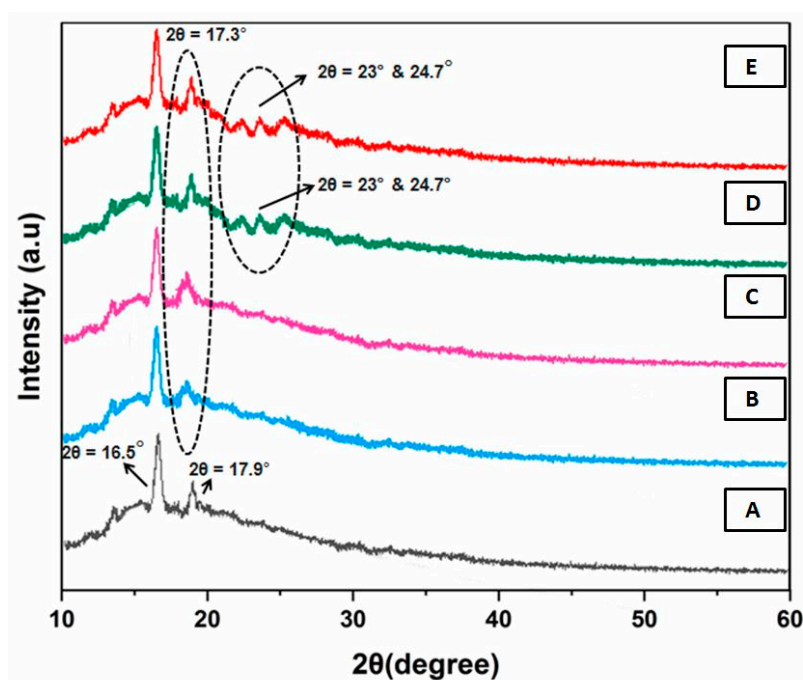


Figure 3. X-ray diffraction values of (A) pure PBAT film, (B) PBAT/5% of GEO composite film, (C) PBAT/10% of GEO composite film, (D) PBAT/10% of GEO/1% of SiO₂ nanocomposite film, (E) PBAT/10% of GEO/3% of SiO₂ nanocomposite film.

Table 2. Percentage of crystallinity of all the prepared film samples.

Film Samples	% Crystallinity = (Area of the Crystalline Peaks/Total Area Peaks) × 100
A	12.31
B	11.56
C	10.46
D	16.31
E	19.74

3.3. Morphological Characterization

The highly magnified microstructures of the pure PBAT, PBAT/GEO, and PBAT/GEO/SiO₂ NPs nanocomposite films are shown in Figure 4 with a 50 μm magnification range using SEM. The SEM morphologies of the pure PBAT film and distinctive PBAT/GEO composite films with low (1%) and high (3%) SiO₂ inclusion concentrations are shown in Figure 4A,B. There were clear changes noticed between the composite films and the control. The control film was smooth and connected in appearance, with no cavities or pores [32]. Though the morphologies of composite films moderately varied from that of the control film, which differed based on the incorporation level of GEO content, the composite films showed rough surfaces, and the even dispersion of GEO droplets in the PBAT polymer matrix was evinced via the respective SEM images in Figure 4C,D. Similar morphologies were noticed within other prepared films, such as agar/GEO, chitosan/GSE, and PBAT/OEO [22,33]. Further, it was noted that the addition of SiO₂NPs in the PBAT/GEO blend decreased the smoothness and caused an increase in the surface roughness of the nanocomposite film [34]. The presence of SiO₂ NPs as dots in Figure 4D,E indicates that nanosilica is present in the PBAT polymer. Figure 4F shows the inner surface microstructure and uniform dispersion of SiO₂ NPs in the PBAT polymer matrix using HRTEM. The purpose of determining the dispersion of oil in the polymer was to understand the effect of oil towards enhancing both film flexibility and antimicrobial efficiency. From the result, it is clearly evident that the greater the oil dispersibility, the greater the film flexibility and antimicrobial effect of the resultant polymer oil mixture is. This dual behavior was shown by means of SEM and TEM analysis, respectively.

3.4. Thermal Analysis

The thermal stability of the PBAT, PBAT/GEO, and PBAT/GEO/SiO₂ nanocomposite films was analyzed, and the outcomes are illustrated in Figure 5. As indicated in the TGA graph, all the films, as well as PBAT, PBAT/GEO, and PBAT/GEO/SiO₂, showed initial weight loss at temperatures of 70–90 °C due to the evaporation of the solvent remaining in the films. Next, major thermal decomposition was seen at about 320–411 °C, which was attributed to the deterioration of aliphatic and aromatic groups in PBAT. The thermal stability of the PBAT film was slightly reduced with the incorporation of GEO. The additional step degradations of PBAT with a low and high concentration of GEO occurred at around 150–170 °C, which was mainly due to the inclusion of GEO, which was combusted during the thermal analysis [35]. As the loading of nanosilica increased, the onset decomposition temperature of PBAT/GEO/1% of SiO₂ NPs and the PBAT/GEO/3% of SiO₂ nanocomposite film increased slightly. This significant improvement in thermal resistance to the existence of SiO₂ NPs in PBAT might be attributed to the formation of confined nanostructure films [35,36]. As a result, the prepared PBAT/GEO/SiO₂ nanocomposite films are recommended for use in food packaging applications requiring strong thermal resistance.

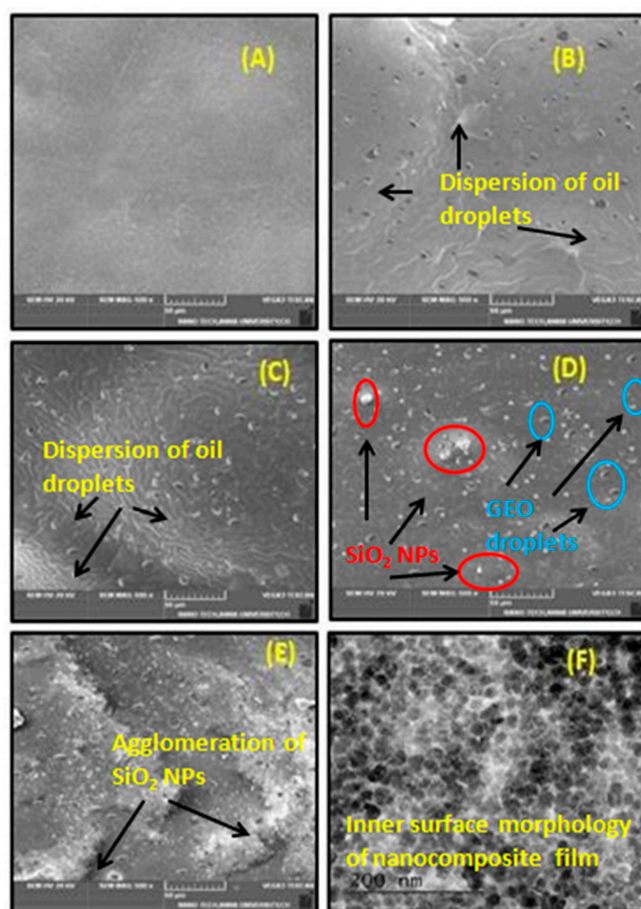


Figure 4. SEM and TEM images of (A) pure PBAT film, (B) PBAT/5% of GEO composite film, (C) PBAT/10% of GEO composite film, (D) PBAT/10% of GEO/1% of SiO₂ nanocomposite film, (E) PBAT/10% of GEO/3% of SiO₂ nanocomposite film, (F) HR-TEM inner surface morphology of nanocomposite film.

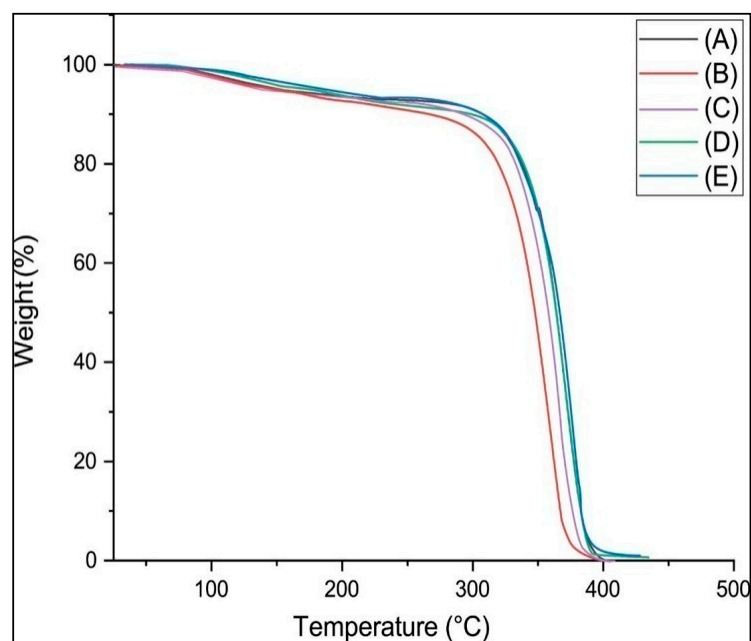


Figure 5. Thermal stability of (A) pure PBAT film, (B) PBAT/5% of GEO composite film, (C) PBAT/10% of GEO composite film, (D) PBAT/10% of GEO/1% of SiO₂ nanocomposite film, (E) PBAT/10% of GEO/3% of SiO₂ nanocomposite film.

3.5. Mechanical Properties

Pure PBAT, PBAT/GEO, and PBAT/GEO/SiO₂ nanocomposite films were tested to obtain the tensile properties such as tensile strength (TS) and elongation at break (EAB), as shown in Table 3. The TS and EAB values of pure PBAT were 35 MPa and 590%, respectively. Soft and highly stretchable molecules were observed in PBAT, which compensated for the good elongation property. It was identified that incorporating 5 and 10 wt% of GEO into the PBAT polymer exhibited maximum EAB values of 612% and 625%, respectively. However, the incorporation of 5 and 10 wt% of GEO decreased the TS values of the PBAT-based films significantly. However, it was noted that the further incorporation of SiO₂NPs into the PBAT admix modified the TS values of the composite films. The addition of 1 and 3% of SiO₂NPs improved the TS values up to 37 and 41 MPa, respectively. These remarkable developments are the cause for the efficient load-sharing capability of silica nanoparticles in the polymer matrix. These nanoparticles evenly transfer the applied load into the matrix, which helps to decrease the stress intensity factor on the inbound microcrack's tip. The enhancement of mechanical properties was achieved by this phenomenon [37].

Table 3. Mechanical properties of composite films.

Composite Samples	Thickness (Microns)	Tensile Strength (MPa)	Elongation at Break (%)	Tensile Modulus (MPa)
A	89	35	590	3.5
B	85	28	612	2.3
C	82	23	625	1.9
D	84	38	203	3.6
E	83	43	595	3.9

This increase in EAB values was due to the presence of GEO, which enhanced the plasticizing effect with the help of glycerol present in the oil and the decreased in TS value, which may have been due to the GEO presence in the PBAT polymer, which weakened the polymer oil interaction, potentially reducing the intermolecular interaction between the PBAT and GEO functional groups. Similarly, Lim et al. [22] and Kanmani et al. [23] reported that the incorporation of essential oil lessened the TS values of the composite films. This was due to the inclusion of essential oil, which damaged the polymer structure. It was also noticed that the addition of SiO₂ NPs to the PBAT/GEO composite film altered the TS and EAB values. The incorporation of 1 and 3 wt% of SiO₂ NPs into the PBAT/GEO blend increased the TS values up to 37 and 41 MPa, respectively. However, the EAB value was reduced to 597 and 581%, respectively, when compared to the films 'B' and 'C'. The presence of SiO₂ NPs in the PBAT polymer matrix contributed to the increase in the TS values of nanocomposite film designations [35].

3.6. Barrier Properties

The oxygen permeability (OP) and WVP of PBAT, PBAT/GEO, and PBAT/GEO/SiO₂ nanocomposite films were estimated (as shown in Figure 6). The control PBAT film had a lower WVTR value (127 g/m²/day) compared with all other PBAT-based films. The water vapor permeability of the films increased with the incorporation of 5 and 10% of GEO into the PBAT films, which may have been due to the loss of inter/intra molecular exchanges among the PBAT matrix, and the presence of hydrophilic GEO induced less crystalline films [36,37]. The hydrophilic nature of the composite film surface was revealed by increasing water contact angle values in Figure 6, whereas the WVP values of nanocomposite film samples 'D' and 'E' increased when evaluated with composite film samples 'B' and 'C', respectively, due to the presence of unpaired double bond oxygen in SiO₂ NPs, which had the highest possibility to react with water and form ortho-silicate [38]. Overall, the WVP values increased for all the prepared films when compared to the pure PBAT film.

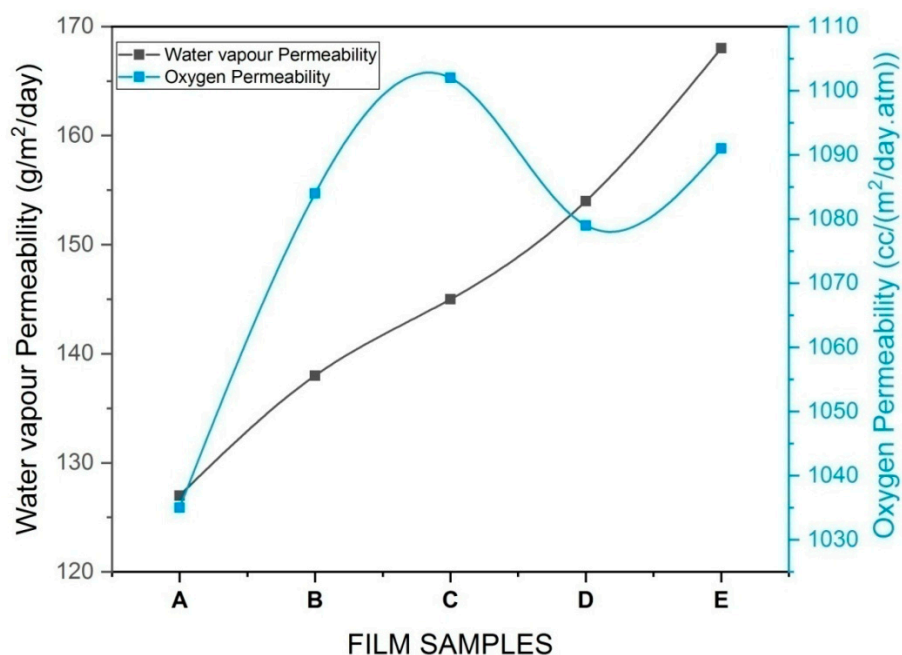


Figure 6. Water vapor and oxygen permeability of (A) pure PBAT film, (B) PBAT/5% of GEO composite film, (C) PBAT/10% of GEO composite film, (D) PBAT/10% of GEO/1% of SiO₂ nanocomposite film, (E) PBAT/10% of GEO/3% of SiO₂ nanocomposite film.

The OP and WVP of PBAT, PBAT/GEO, and PBAT/GEO/SiO₂ nanocomposite films were determined (refer to Figure 6). The control PBAT film had a lower OTR value (1035.1 cc/m²·day·atm) compared with all other PBAT-based films. The oxygen permeability of the films increased with the incorporation of 5 and 10% of GEO into the PBAT films, which may have been due to the existence of flavonoids and phenolic compounds in GEO which increased the OP values and reduced the polarity of the PBAT/GEO composite films [37]. The OP values of nanocomposite films 'D' and 'E' were slightly lower than those of composite films 'B' and 'C'. The addition of SiO₂ NPs and its oxygen with an unpaired double bond altered the film's crystallinity and formed a complex path for oxygen permeation. Twisted gas pathways were observed due to the inclusion of NPs in flexible packaging materials [26]. The gas permeabilities of the films were affected by crystallinity, with increased crystallinity decreasing oxygen and water vapor permeability [38]. Finally, it was concluded that there was an overall rise in OP values in all the fabricated films in comparison with the pure PBAT film. The results were compared with similar studies reported in the field of active packaging [39–41]. Additionally, it was inferred that similar results were observed with the increased addition of GSE into different biopolymers such as chitosan, Gelidium corneum, and gelatin film. Higher WVP and OP values are prerequisites for fresh fruits and vegetables packaging applications. Hence, they are recommended for the packaging of fresh agricultural produce where a high respiration rate (RR) is realized.

3.7. Water Contact Angle Measurement

The water contact angle (WCA) of PBAT, PBAT/GEO, and PBAT/GEO/SiO₂ nanocomposite films is illustrated in Figure 7. The WCA represents the film's contact with liquids, and it is viewed as an important property for the film's application in food packaging. The PBAT, PBAT/GEO, and PBAT/GEO/SiO₂ nanocomposite films had WCA values of 66.1°, 62.3°, 59.4°, 56.6°, and 53°, respectively.

The WCA of the composite films was less than 65°, which produces hydrophilic films and which was similar to earlier reports (PLA/PBAT/GEO, PLA/PBAT, and PLA/PBAT/CO-blended films) [25,28,32]. The WCA values of the pure PBAT, PBAT/GEO, and PBAT/GEO/SiO₂ nanocomposite films reduced marginally after the addition of GEO. The decrease in

the WCA of the PBAT-based composite films was primarily attributed to the addition of GEO and SiO₂ NPs [22,24].

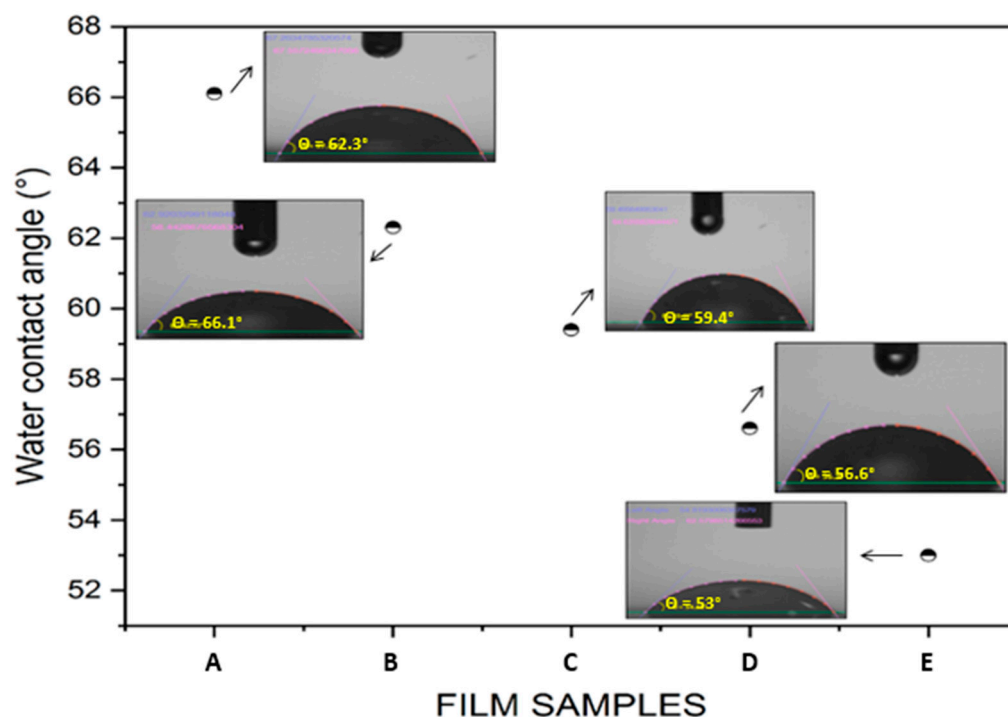


Figure 7. Water contact angle of (A) pure PBAT film, (B) PBAT/5% of GEO composite film, (C) PBAT/10% of GEO composite film, (D) PBAT/10% of GEO/1% of SiO₂ nanocomposite film, (E) PBAT/10% of GEO/3% of SiO₂ nanocomposite film.

3.8. Film Color and Opacity

Table 4 shows the surface color values and opacity of PBAT, PBAT/GEO, and PBAT/GEO/SiO₂. Using Equation (1), the total color difference in all the prepared film samples was computed.

$$\Delta E = [(\Delta L)^2 + (\Delta a)^2 + (\Delta b)^2]^{0.5} \quad (1)$$

Table 4. Surface color values of PBAT/PBAT/GEO and PBAT/GEO/SiO₂ nanocomposite films.

Film Samples	Lightness (L*)	Redness, Greenness (a*)	Yellowness, Blueness (b*)	Total Color Difference (ΔE)	Opacity (%)
A	90.5	−1.45	5.13	NA	46.7
B	86.24	−1.19	4.28	4.35	42.3
C	86.53	−1.09	5.83	4.04	37.6
D	84.85	−1.31	6.10	5.73	45.2
E	82.80	−1.88	6.03	7.76	47.1

In terms of appearance, the color of packaging film influences consumer behavior. All of the prepared film samples were visually inspected for cracks and pinholes, and the film with an even thickness was chosen for surface color measurement. By choosing the color of pure PBAT as the reference standard, the effect of GEO and SiO₂ NPs on all the prepared PBAT-based films was investigated. The surface color and opacity values of PBAT blended with GEO and SiO₂ NPs are presented in Table 4. When compared to pure PBAT, the composite film containing GEO has more yellowness (b-value). The increase in yellow color in the composite films is caused by the carotenoid compound present in the GEO-containing PBAT film, and the total color difference (E) increases as the percentage

of GEO increases [36]. Shankar et al. [27] also recorded the increased yellowness (b-value) value of PLA/PBAT-blended films containing GEO. Corrales et al. [37] also found a similar increase in yellowness in starch/GSE-based composite films. Wang and Rhim et al. [25] also recorded an increase in the yellowness (b-value) of PLA/LDPE films after GSE addition.

The opacity value of plain PBAT was 46.7%, whereas the measured opacity values of PBAT/5 and 10% GEO were 42.3% and 37.6%, respectively. The dispersed GEO in the PBAT film improved surface smoothness and brightness, increasing the reflectance value. When compared to pure PBAT, the PBAT/GEO/SiO₂ nanocomposite film had a higher percentage of opacity value. This was due to light scattering on the film surface caused by tiny drops of GEO dispersion in the PBAT polymer, as well as the presence of SiO₂NPs, which block the passage of light. As a result, this property of the PBAT nanocomposite material may be best suited for food preservation because it reduces the photo-oxidation of organic compounds [38].

3.9. Antimicrobial Activity

The antimicrobial activities of the pure PBAT, PBAT/GEO, and PBAT/GEO/SiO₂ nanocomposite films that were evaluated against microbial strains of *S.aureus* and *E.coli* are shown in Figure 8. Figure 8 and Table 5 illustrate the antimicrobial activities of pure PBAT, PBAT/GEO, and PBAT/GEO/SiO₂ nanocomposite films against microbial strains such as *S.aureus* and *E.coli*. As expected, GEO-incorporated PBAT composite films revealed sound inhibitory activities against Gram-positive and negative microorganisms. The pure PBAT film sample 'A' had no zone of inhibition, indicating poor antibacterial resistance against both positive and negative microorganisms. However, the antimicrobial activity of the composite films prepared with GEO and the nanocomposite film with SiO₂ NPs was enhanced [39]. It is also important to note that the zone of inhibition was detected in film samples B, C, D, and E in comparison to pure PBAT. The antimicrobial effect of active GEO, as well as the SiO₂ NPs in the PBAT matrix, was responsible for this improvement. The antibacterial properties of GEO, which include flavonoids, phenolic acid, tocopherol, and other antimicrobial compounds, were also responsible for this improvement [40,41]. Similarly, the inbuilt antimicrobial activity of SiO₂NPs in nanocomposite film samples 'D' and 'E' was found to have a stronger inhibitory effect than in the composite films 'B' and 'C'. As a result, it was considered that incorporating GEO and SiO₂NPs would be more effective in preventing pathogenic microorganisms. The antibacterial properties were confirmed and justified by the previous research work with PBAT/SiO₂ and PVA/SiO₂ composite films [42,43]. The antibacterial properties of SiO₂NPs were found to be proportional to their total surface area. Smaller particles with a higher surface-to-volume ratio had higher antibacterial activity [44].

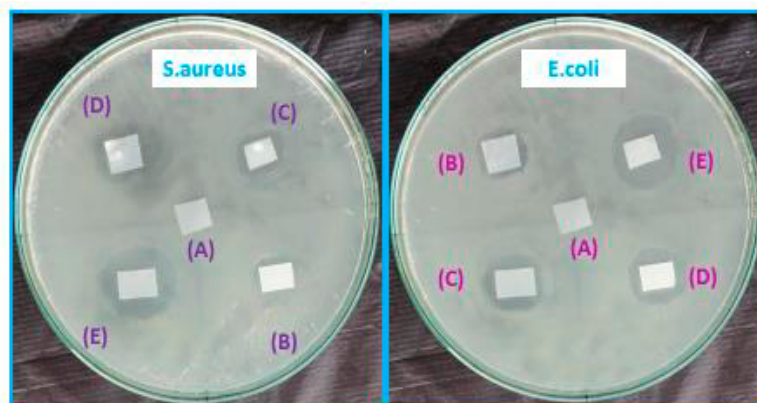


Figure 8. Antimicrobial activities of (A) pure PBAT film, (B) PBAT/5% of GEO composite film, (C) PBAT/10% of GEO composite film, (D) PBAT/10% of GEO/1% of SiO₂ nanocomposite film, (E) PBAT/10% of GEO/3% of SiO₂ nanocomposite film.

Table 5. Antimicrobial activity of prepared PBAT, PBAT/GEO, and PBAT/GEO/SiO₂ nanocomposite films.

Film Samples	Zone Inhibition (mm)	
	<i>E. coli</i>	<i>S. aureus</i>
A	ND	ND
B	7	5
C	9	7
D	12	9
E	14	11

ND—not detected.

4. Conclusions

The PBAT-based composite and nanocomposite films were successfully prepared via the solution casting technique. The films were prepared by combining PBAT as the base polymer with GEO and SiO₂ NPs. The film morphological results showed a more homogeneous PBAT/GEO blend with the good dispersion of SiO₂ NPs in the PBAT matrix. The FT-IR spectral results and diffraction peaks of all of the prepared film samples proved the effective miscibility of GEO and the even dispersion of SiO₂ NPs in the biobased PBAT polymer. According to the TGA results, the nanocomposite film containing 3 wt% SiO₂ NPs had the highest thermal stability. The mechanical properties of composite film samples 'B' and 'C' showed an improvement in EAB values when compared to the plain PBAT polymer, and nanocomposite films containing SiO₂ NPs increased the TS values. The oxygen and water vapor permeability of composite films 'B' and 'C' were higher when compared to nanocomposite films containing SiO₂ NPs 'D' and 'E,' but all of the film samples except pure PBAT exhibited poor barrier properties against oxygen and water permeability. The antimicrobial results showed that the presence of GEO and SiO₂ NPs contributed to enhanced resistance against both Gram-positive and Gram-negative microbes. Thus, incorporating GEO into PBAT composite films improved elongation at break, film transparency, and antibacterial activity, whereas incorporating SiO₂ NPs improved nanocomposite film tensile strength, opacity, and thermal stability. These mechanically strengthened, antibacterial-resistant, and thermally stable biopolymer-based composite and nanocomposite films were found to be highly suitable materials in active food packaging applications.

Author Contributions: T.T.—methodology, experimental work, and writing. J.K.—supervision and language correction, S.A.—technical evaluation, P.S.—writing, review and editing. All authors have read and agreed to the published version of the manuscript.

Funding: This research received no external funding.

Institutional Review Board Statement: Not applicable.

Informed Consent Statement: Not applicable.

Data Availability Statement: Not applicable.

Conflicts of Interest: The authors declare no conflict of interest.

References

- Hailu, M.; Workneh, T.S.; Belew, D. Effect of packaging materials on shelf life and quality of banana cultivars (*Musa* spp.). *J. Food Sci. Technol.* **2012**, *51*, 2947–2963. [[CrossRef](#)] [[PubMed](#)]
- Radusin, T.; Tomšik, A.; Šarić, L.; Ristić, I.; Baschetti, M.G.; Minelli, M.; Novaković, A. Hybrid Pla/wild garlic antimicrobial composite films for food packaging application. *Polym. Compos.* **2018**, *40*, 893–900. [[CrossRef](#)]
- Didone, M.; Saxena, P.; Brilhuis-Meijer, E.; Tosello, G.; Bissacco, G.; Mcaloone, T.C.; Pigosso, D.C.A.; Howard, T.J. Moulded pulp manufacturing: Overview and prospects for the process technology. *Packag. Technol. Sci.* **2017**, *30*, 231–249. [[CrossRef](#)]
- Qian, M.; Liu, D.; Zhang, X.; Yin, Z.; Ismail, B.B.; Ye, X.; Guo, M. A review of active packaging in bakery products: Applications and future trends. *Trends Food Sci. Technol.* **2021**, *114*, 459–471. [[CrossRef](#)]
- Wang, J.; Euring, M.; Ostendorf, K.; Zhang, K. Biobased materials for food packaging. *J. Bioresour. Bioprod.* **2021**, *7*, 1–13. [[CrossRef](#)]

6. Garavand, F.; Cacciotti, I.; Vahedikia, N.; Rehman, A.; Tarhan, Ö.; Akbari-Alavijeh, S.; Shaddel, R.; Rashidinejad, A.; Nejatian, M.; Jafarzadeh, S. A comprehensive review on the nanocomposites loaded with chitosan nanoparticles for food packaging. *Crit. Rev. Food Sci. Nutr.* **2020**, *62*, 1383–1416. [[CrossRef](#)]
7. Saxena, P.; Bissacco, G.; Meinert, K.Æ.; Bedka, F.J. Mold design and fabrication for production of thermoformed paper-based packaging products. *J. Manuf. Process.* **2020**, *58*, 311–321. [[CrossRef](#)]
8. Reichert, C.L.; Bugnicourt, E.; Coltelli, M.-B.; Cinelli, P.; Lazzeri, A.; Canesi, I.; Braca, F.; Martínez, B.M.; Alonso, R.; Agostinis, L.; et al. Bio-Based Packaging: Materials, Modifications, Industrial Applications and Sustainability. *Polymers* **2020**, *12*, 1558. [[CrossRef](#)]
9. Chausali, N.; Saxena, J.; Prasad, R. Recent trends in nanotechnology applications of bio-based packaging. *J. Agric. Food Res.* **2021**, *7*, 100257. [[CrossRef](#)]
10. Azeredo, H.M.C.; Rosa, M.F.; Mattoso, L.H.C. Nanocellulose in bio-based food packaging applications. *Ind. Crops Prod.* **2017**, *97*, 664–671. [[CrossRef](#)]
11. Niranjana Prabhu, T.; Prashantha, K. A review on present status and future challenges of starch based polymer films and their composites in food packaging applications. *Polym. Compos.* **2018**, *39*, 2499–2522. [[CrossRef](#)]
12. Varshney, S.; Mishra, N.; Gupta, M. Progress in nanocellulose and its polymer based composites: A review on processing, characterization, and applications. *Polym. Compos.* **2021**, *42*, 3660–3686. [[CrossRef](#)]
13. Zhuang, C.; Tao, F.; Cui, Y. Eco-friendly biorefractory films of gelatin and TEMPO-oxidized cellulose ester for food packaging application. *J. Sci. Food Agric.* **2017**, *97*, 3384–3395. [[CrossRef](#)] [[PubMed](#)]
14. Subbuvel, M.; Kavan, P. Preparation and characterization of polylactic acid/fenugreek essential oil/curcumin composite films for food packaging applications. *Int. J. Biol. Macromol.* **2021**, *194*, 470–483. [[CrossRef](#)] [[PubMed](#)]
15. Yao, Q.; Song, Z.; Li, J.; Zhang, L. Micromorphology, mechanical, crystallization and permeability properties analysis of HA/PBAT/PLA (HA, hydroxyapatite; PBAT, poly(butylene adipate-co-butylene terephthalate); PLA, polylactide) degradability packaging films. *Polym. Int.* **2019**, *69*, 301–307. [[CrossRef](#)]
16. Lu, W.; Cui, R.; Zhu, B.; Qin, Y.; Cheng, G.; Li, L.; Yuan, M. Influence of clove essential oil immobilized in mesoporous silica nanoparticles on the functional properties of poly (lactic acid) biocomposite food packaging film. *J. Mater. Res. Technol.* **2021**, *11*, 1152–1161. [[CrossRef](#)]
17. Thiyagu, T.T.; Rajeswari, N. Effect of nanosilica and neem tree oil on antimicrobial, thermal, mechanical and electrical insulate of biodegradable composite film. *Mater. Res. Express* **2019**, *6*, 095410. [[CrossRef](#)]
18. Sharma, B.; Malik, P.; Jain, P. Biopolymer reinforced nanocomposites: A comprehensive review. *Mater. Today Commun.* **2018**, *16*, 353–363. [[CrossRef](#)]
19. Priyadarshi, R.; Roy, S.; Ghosh, T.; Biswas, D.; Rhim, J.W. Antimicrobial nanofillers reinforced biopolymer composite films for active food packaging applications—a review. *Sustain. Mater. Technol.* **2021**, *3*, e00353. [[CrossRef](#)]
20. Luo, Q.; Hossen, A.; Zeng, Y.; Dai, J.; Li, S.; Qin, W.; Liu, Y. Gelatin-based composite films and their application in food packaging: A review. *J. Food Eng.* **2021**, *313*, 110762. [[CrossRef](#)]
21. Lyu, J.S.; Lee, J.-S.; Han, J. Development of a biodegradable polycaprolactone film incorporated with an antimicrobial agent via an extrusion process. *Sci. Rep.* **2019**, *9*, 20236. [[CrossRef](#)] [[PubMed](#)]
22. Lim, G.-O.; Jang, S.-A.; Bin Song, K. Physical and antimicrobial properties of *Gelidium corneum*/nano-clay composite film containing grapefruit seed extract or thymol. *J. Food Eng.* **2010**, *98*, 415–420. [[CrossRef](#)]
23. Kanmani, P.; Rhim, J.-W. Development and characterization of carrageenan/grapefruit seed extract composite films for active packaging. *Int. J. Biol. Macromol.* **2014**, *68*, 258–266. [[CrossRef](#)]
24. Rubilar, J.F.; Cruz, R.M.; Khmelinskii, I.; Vieira, M.C. Effect of antioxidant and optimal antimicrobial mixtures of carvacrol, grape seed extract and chitosan on different spoilage microorganisms and their application as coatings on different food matrices. *Int. J. Food Stud.* **2013**, *2*, 22–38. [[CrossRef](#)]
25. Wang, L.F.; Rhim, J.W. Grapefruit seed extract incorporated antimicrobial LDPE and PLA films: Effect of type of polymer matrix. *LWT* **2016**, *74*, 338–345. [[CrossRef](#)]
26. Garavand, F.; Rouhi, M.; Razavi, S.H.; Cacciotti, I.; Mohammadi, R. Improving the integrity of natural biopolymer films used in food packaging by crosslinking approach: A review. *Int. J. Biol. Macromol.* **2017**, *104*, 687–707. [[CrossRef](#)]
27. Shankar, S.; Rhim, J.W. Preparation of antibacterial poly (lactide)/poly (butylene adipate-co-terephthalate) composite films incorporated with grapefruit seed extract. *Int. J. Biol. Macromol.* **2018**, *120*, 846–852. [[CrossRef](#)]
28. Sanuja, S.; Agalya, A.; Umopathy, M.J. Studies on magnesium oxide reinforced chitosan bionanocomposite incorporated with clove oil for active food packaging application. *Int. J. Polym. Mater. Polym. Biomater.* **2014**, *63*, 733–740. [[CrossRef](#)]
29. Aji, A.L.; Praseptianga, D.; Rochima, E.; Joni, I.M.; Panatarani, C. Optical transparency and mechanical properties of semi-refined iota carrageenan film reinforced with SiO₂ as food packaging material. *AIP Conf. Proc.* **2018**, *1927*, 030039.
30. Chivrac, F.; Pollet, E.; Avérous, L. Nonisothermal crystallization behavior of poly (butylene adipate-co-terephthalate)/clay nano-biocomposites. *J. Polym. Sci. Part B Polym. Phys.* **2007**, *45*, 1503–1510. [[CrossRef](#)]
31. Gadang, V.; Hettiarachchy, N.; Johnson, M.; Owens, C. Evaluation of Antibacterial Activity of Whey Protein Isolate Coating Incorporated with Nisin, Grape Seed Extract, Malic Acid, and EDTA on a Turkey Frankfurter System. *J. Food Sci.* **2008**, *73*, M389–M394. [[CrossRef](#)] [[PubMed](#)]

32. Figueroa-Lopez, K.J.; Andrade-Mahecha, M.M.; Torres-Vargas, O.L. Development of Antimicrobial Biocomposite Films to Preserve the Quality of Bread. *Molecules* **2018**, *23*, 212. [[CrossRef](#)] [[PubMed](#)]
33. Martínez-Castañón, G.A.; Niño-Martínez, N.; Martínez-Gutiérrez, F.; Martínez-Mendoza, J.R.; Ruiz, F. Synthesis and antibacterial activity of silver nanoparticles with different sizes. *J. Nanoparticle Res.* **2008**, *10*, 1343–1348. [[CrossRef](#)]
34. Venkatesan, R.; Thiyagu, T.T.; Rajeswari, N. Zinc composite materials and food packaging. *Compos. Mater. Food Packag.* **2018**, 153–175. [[CrossRef](#)]
35. Venkatesan, R.; Rajeswari, N. Nanosilica-reinforced poly (butylene adipate-co-terephthalate) nanocomposites: Preparation, characterization and properties. *Polym. Bull.* **2019**, *76*, 4785–4801. [[CrossRef](#)]
36. Raja, V.; Natesan, R.; Thiyagu, T. Preparation and Mechanical Properties of Poly (butylene adipate-co-terephthalate) Polyvinyl Alcohol/SiO₂ Nanocomposite Films for Packaging Applications. *J. Polym. Mater.* **2015**, *32*, 93.
37. Corrales, M.; Han, J.H.; Tauscher, B. Antimicrobial properties of grape seed extracts and their effectiveness after incorporation into pea starch films. *Int. J. Food Sci. Technol.* **2009**, *44*, 425–433. [[CrossRef](#)]
38. Balan, G.C.; Paulo, A.F.; Correa, L.G.; Alvim, I.D.; Ueno, C.T.; Coelho, A.R.; Ströher, G.R.; Yamashita, F.; Sakanaka, L.S.; Shirai, M.A. Production of Wheat Flour/PBAT Active Films Incorporated with Oregano Oil Microparticles and Its Application in Fresh Pastry Conservation. *Food Bioprocess Technol.* **2021**, *14*, 1587–1599. [[CrossRef](#)]
39. Sharma, C.; Dhiman, R.; Rokana, N.; Panwar, H. Nanotechnology: An Untapped Resource for Food Packaging. *Front. Microbiol.* **2017**, *8*, 1735. [[CrossRef](#)]
40. Hajizadeh, H.; Peighambaroust, S.J.; Peighambaroust, S.H.; Peressini, D. Physical, mechanical, and antibacterial characteristics of bio-nanocomposite films loaded with Ag-modified SiO₂ and TiO₂ nanoparticles. *J. Food Sci.* **2020**, *85*, 1193–1202. [[CrossRef](#)]
41. Sharma, S.; Barkauskaite, S.; Jaiswal, S.; Duffy, B.; Jaiswal, A.K. Development of essential oil incorporated active film based on biodegradable blends of poly (lactide)/poly (butylene adipate-co-terephthalate) for food packaging application. *J. Packag. Technol. Res.* **2020**, *4*, 235–245. [[CrossRef](#)]
42. Rubilar, J.F.; Cruz, R.M.S.; Silva, H.D.; Vicente, A.A.; Khmelinskii, I.; Vieira, M.C. Physico-mechanical properties of chitosan films with carvacrol and grape seed extract. *J. Food Eng.* **2013**, *115*, 466–474. [[CrossRef](#)]
43. Thiyagu, T.T.; Gokilakrishnan, G.; Uvaraja, V.C.; Maridurai, T.; Prakash, V.R. Effect of SiO₂/TiO₂ and ZnO nanoparticle on cardanol oil compatibilized PLA/PBAT biocomposite packaging film. *Silicon* **2022**, *14*, 3795–3808. [[CrossRef](#)]
44. Cho, K.H.; Park, J.E.; Osaka, T.; Park, S.G. The study of antimicrobial activity and preservative effects of nanosilver ingredient. *Electrochim. Acta* **2005**, *51*, 956–960. [[CrossRef](#)]